High-Frequency MW-class Coaxial Gyrotron Cavities Operating at the Second Cyclotron Harmonic

Ioannis G. Chelis, Konstantinos A. Avramidis, Dimitrios V. Peponis, Zisis C. Ioannidis, *Member, IEEE*, George P. Latsas, Stefan Illy, John Jelonnek, *Senior Member, IEEE*, and Ioannis G. Tigelis, *Senior Member, IEEE*

***Abstract*— Second-harmonic operation of gyrotron oscillators offers the possibility to generate millimeter and submillimeter radiation at half the value of the magnetic field required for operation at the fundamental cyclotron frequency (first harmonic). However, being inherently weaker than the interaction at the first harmonic, high-power second-harmonic continuous-wave (CW) operation employing high-order modes faces strong mode competition from the first-harmonic competing modes. It is shown that coaxial cavities with a corrugated insert allow to drastically enhance the mode selectivity at the second harmonic and suppress the first-harmonic competitors in MW-class gyrotrons. Detailed design considerations for coaxial cavities are presented and specific cavity designs for various candidate operating modes are given. We demonstrate numerically, with multimode interaction simulations, stable second-harmonic CW generation of 2 MW output power at 170 GHz and 0.7 MW at 280 GHz, using high-order modes with eigenvalues >100. The presented results show the possibility to design second-harmonic gyrotrons with cost-effective magnet systems and achieve MW-class CW operation at frequencies above 250 GHz.**

***Index Terms*— Coaxial cavities, corrugated insert, gyrotron, mode competition, second harmonic.**

Manuscript received 20 September 2023; revised 1 December 2023 and 29 December 2023; accepted 16 January 2024. Date of publication 1 February 2024; date of current version 1 March 2024. This work has been carried out within the framework of the EUROfusion Consortium, funded by the European Union via the Euratom Research and Training Programme (Grant Agreement No. 101052200—EUROfusion). Views and opinions expressed are however those of the author(s) only and do not necessarily reflect those of the European Union or the European Commission. Neither the European Union nor the European Commission can be held responsible for them. The publication of the article in OA mode was financially supported by HEAL-Link. The review of this article was arranged by Editor J. Feng. *(Corresponding author: Ioannis G. Chelis.)*

Ioannis G. Chelis, Konstantinos A. Avramidis, Dimitrios V. Peponis, George P. Latsas, and Ioannis G. Tigelis are with the Department of Physics, National and Kapodistrian University of Athens, 157 84 Athens, Greece (e-mail: ichelis@phys.uoa.gr).

Zisis C. Ioannidis is with the Department of Aerospace Science and Technology, National and Kapodistrian University of Athens, Euripus Campus, 344 00 Psachna, Greece.

Stefan Illy and John Jelonnek are with the Institute for Pulsed Power and Microwave Technology, Karlsruhe Institute of Technology, 76131 Karlsruhe, Germany.

Color versions of one or more figures in this article are available at https://doi.org/10.1109/TED.2024.3356472.

Digital Object Identifier 10.1109/TED.2024.3356472

I. Introduction

THE gyrotron oscillator is the main microwave source capable of delivering RF power in the order of hundreds of kilowatts at millimeter and even submillimeter frequencies. High-power continuous-wave (CW) gyrotrons are primarily used in fusion devices (Tokamaks and Stellarators) for electron cyclotron resonance heating (ECRH) and electron cyclotron current drive (ECCD) [1]. With the emergence of high-field tokamaks and the so-called high-field path to fusion energy [2], the need for MW-class gyrotrons operating at higher frequencies >250 GHz is becoming timely [3]. Such high-frequency high-power gyrotrons are also attractive for fusion plasma diagnostics based on collective Thomson scattering (CTS), since the submillimeter band exhibits low noise from electron cyclotron emission [4] and the high output power improves the system's signal-to-noise ratio. However, operating a MW-class gyrotron at such high frequencies requires increased magnetostatic field values (>10 T), which are currently not possible to produce cost-effectively from superconducting magnet systems with large bore-hole.

In particular, the maximum field limit for the current superconducting technology based on NbTi is around 9.5 T. For higher magnetic field values, one has to switch to Nb_3Sn material, which is at least one order of magnitude more expensive compared to NbTi. In addition, it requires special treatment after winding and is much more sensitive and brittle. All this make the whole magnet system more expensive at least by a factor of two. It is estimated that a first-harmonic gyrotron at around 250 GHz or above would require such an expensive magnet based on Nb_3Sn.

One way to halve the required magnetostatic field value and maintain cost-effectiveness is to operate the gyrotron at the second cyclotron harmonic. Second-harmonic gyrotrons at higher frequencies in CW or pulsed operation have been used mostly at low and medium power for dynamic nuclear polarization (DNP)-enhanced nuclear magnetic resonance (NMR) spectroscopy [5], [6], [7], [8] or for plasma CTS diagnostics [9], but their capability for MW-class CW operation has not been thoroughly investigated yet.

With the increase of the operating frequency and output power, the ohmic losses at the walls of the gyrotron cavity

rise significantly and large cavities operating with high-order modes are required to maintain the ohmic loading at acceptable levels. As a result, the mode spectrum becomes denser and stable single-mode operation is impeded by mode competition. Furthermore, since the interaction at the second harmonic is inherently weaker than the interaction at the fundamental for a given field amplitude level, the operating second-harmonic mode faces strong mode competition from its first-harmonic competitors. For example, in [10], the concept of injection locking was employed as a means for enhancing mode selectivity and exciting, in simulation, the second-harmonic mode $TE_{34,14}$ up to 0.9 MW at 230 GHz with an external signal of 50 kW. However, this approach exhibits increased complexity, since it requires an additional source of medium-power radiation of the same frequency, which also needs to be highly stable.

A simpler way to enhance the mode selectivity of high-power gyrotron cavities is to use a coaxial cavity with a corrugated inner conductor [11], [12]. The tapered insert affects the competing modes of lower caustic radii and decreases their quality factor. A coaxial cavity with a corrugated insert has been successfully used to generate, in the experiment, more than 2 MW of output power at 170 GHz based on the $TE_{34,19}$ mode at the fundamental cyclotron frequency [13]. Second-harmonic coaxial gyrotron cavities with a corrugated insert have been investigated theoretically at submillimeter frequencies for medium output-power level in [14], where a design for a 100 kW CW 340 GHz cavity is presented, as well as for DNP-NMR and CTS diagnostics applications in [15] and [16], respectively. Recently, a design for a high-power second-harmonic coaxial cavity operating at 170 GHz with $TE_{34,19}$ was presented, showing 1.3 MW of output power [17].

Although the coaxial technology is very promising for enhancing mode selectivity and also reduces significantly the space-charge depression, it is accompanied by a certain complexity and some uncertainties regarding the cooling of the coaxial insert, the induced vibrations because of the cooling, and the precise alignment of the insert. In particular, it is estimated that the cooled coaxial insert can withstand a reduced ohmic loading compared to the outer cavity wall as will be discussed in the next Section. In addition, the water flow can induce unwanted vibrations, which can degrade significantly the RF behavior of the cavity. Finally, the insert should be precisely aligned in the cavity within acceptable tolerances. As the coaxial gyrotron experiments up to now have been performed only in short pulses, the above aspects remain to be validated in CW conditions, too.

In this work, we present a systematic investigation of MW-class second-harmonic CW coaxial cavities employing a corrugated insert to suppress the first-harmonic competitors. The rest of the manuscript is organized as follows. In Section II, we focus on second-harmonic operation at 170 GHz and discuss various design considerations that allow achieving MW-class output power. In Section III, we consider additional second-harmonic operating modes and investigate possible differences with respect to mode competition. In Section IV, based on the developed strategies, we present a MW-class cavity design for 280 GHz. Finally, the results are discussed and concluded in Section V.

II. Design Considerations for MW-class Second-Harmonic Operation

A. General Considerations

The aim of our theoretical investigation is to examine the possibility of using high-order modes in order to achieve MW-class second-harmonic operation at very high frequencies >250 GHz. For each selected frequency, we pursue single-frequency operation only at the second-harmonic mode. In this section, we first focus on operation at 170 GHz. At this frequency, a possible experimental demonstration of MW-class operation at the second harmonic is more straightforward, since the coaxial technology has been already used at 170 GHz [13]. In addition, many first-harmonic cavity designs exist for comparison at this frequency, so we first focus on 170 GHz to develop design guidelines and general principles. These will be used in Section IV to derive a cavity design for 280 GHz.

For operation at 170 GHz, we set the target to 2 MW for the output power (as achieved in [13] at the fundamental harmonic) and to ≥20% for the electronic efficiency η_{el}. The latter target seems relatively low for fusion applications, however, the 20%–25% electronic efficiency level could be increased to 55%–62% of total efficiency through the use of a multistage depressed collector (assuming a collector efficiency of 80%) [18]. The reduced electronic efficiency compared to the typical electronic efficiency of about 35% is an unavoidable compromise at the second harmonic, since the interaction at higher harmonics is inherently weaker than the interaction at the fundamental for a given RF field amplitude. That is, to achieve the same efficiency with second-harmonic interaction, a much higher RF field in the cavity is required, resulting in prohibitively high ohmic wall loading [14].

The cavity design should be compatible with CW operation, i.e., the ohmic loading at the outer wall $\rho_{out,max}$ should not exceed the current technological cooling limit, for which we assume here a conservative value of 2.2 kW/cm^2. For our target of 2 MW at 170 GHz, this constraint implies the use of high-order modes with an eigenvalue >100 (as indicated by (8) in [14]). For the inner conductor, the ohmic loading limit is typically set to 10% of $\rho_{out,max}$, i.e., 0.22 kW/cm^2. However, according to recent studies, this value is quite conservative and a higher limit of up to 0.39 kW/cm^2 is proposed [19]. The above limitations are observed in this article. Note that for the ohmic loss calculations in this work, we use CW-compatible conductivity values. In particular, for the outer wall, we use a pessimistic effective conductivity value of 1.73×10^7 S/m corresponding to a correction factor of 1.8 with respect to the conductivity of ideal smooth copper at room temperature. For the coaxial insert, we have used a higher effective conductivity value of 2.77×10^7 S/m, in order to take into account the reduced temperature, compared to the outer wall, expected at the insert. This estimated effective conductivity value assumes a copper surface roughness of 0.05 mm, an RF frequency of 280 GHz, and a coaxial insert temperature at the level of 175°. This is the maximum expected temperature at the insert, as calculated in [19]. All cavity interaction simulations have been performed with the European time-dependent

multimode code EURIDICE [20] and typical electron beam spreads have been considered (i.e., a 5% rms spread in electron velocity ratio α, a 0.01% rms spread in electron kinetic energy, and a uniform guiding center spread of two Larmor radii).

In this study, we will consider the concept of a highly conductive insert with longitudinal surface impedance corrugations [11]. The corrugated insert affects the competing modes that have a caustic radius comparable to the insert radius or lower and increases their diffraction losses. The corrugation depth d is chosen as $d/\lambda_{c0} = 0.4$, as proposed in [14], where λ_{c0} is the cutoff wavelength of the operating second-harmonic mode. With this choice, the first-harmonic competitors "see" a corrugation depth of $d/\lambda_{c0} \cong 0.2$ and their eigenvalue curves versus the ratio of the outer wall radius to the insert radius become monotonic with a negative slope [12], [14]. As a result, with a down-tapered inner rod, their axial wavenumber increases toward the cavity output and their diffractive quality factor decreases significantly. The eigenvalue curves of the second-harmonic modes may exhibit a region of small positive slope, which may increase slightly their Q factor, but this is not necessarily a negative effect as this increase also occurs for the operating mode.

Initial information on mode competition can be obtained from the generalized coupling factor of each mode defined as follows:

$$G^2_{mp,s}(k_\perp R_b) = \left[J_{m-s}(k_\perp R_b) - \frac{J'_m(\chi_{mp})}{Y'_m(\chi_{mp})} Y_{m-s}(k_\perp R_b) \right]^2 \cdot s^2 C^2_{mp} \left[\left(\frac{s}{2}\right)^s \frac{u^s_\perp}{(s-1)!} \right]^2 \quad (1)$$

where χ_{mp} is the eigenvalue of the mode, $k_\perp$ is the transverse wavenumber, R_b is the beam radius, $u_\perp$ is the dimensionless transverse momentum, and $J(x)$, $Y(x)$ are the Bessel functions of the first and second kind, respectively. The first term corresponds to the well-known coupling factor for coaxial cavities, which depends on the radial positioning of the beam. The factor C^2_{mp} denotes the squared normalization coefficient of each mode and is given by (3) in [14]. We include C^2_{mp} in the definition, since it allows us to compare modes with different transverse structures. In the case of a conventional cavity without an inner rod, the normalization coefficient and the coupling factor are simplified accordingly. We also include the factor s^2, where the integer s is the harmonic number; $s = 1$ for interaction at the first harmonic. This factor reflects the increased diffractive quality factor of second-harmonic modes by a factor of around four due to their double frequency. The last term in brackets, which depends on the transverse momentum and the harmonic number s, expresses the dependence of the interaction strength on the harmonic number. This term has been extracted from (16) and (17) of [21], which give an approximate fixed-field analytic expression for the starting current in harmonic gyrotrons. Our generalized definition of the coupling factor is an approximate figure of merit that illustrates the competition between the different modes, and allows to compare modes of different harmonic number, too.

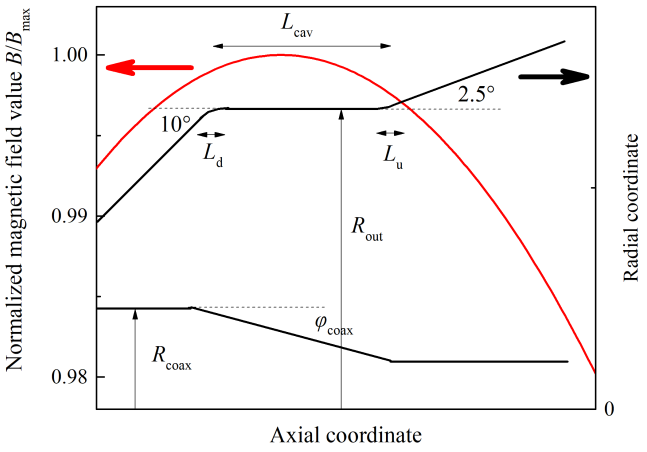

Fig. 1. Magnetic field profile (normalized to unity) and the general coaxial geometry considered (outer wall and corrugated inner rod).

B. Design Considerations With Respect to Coaxial Insert Geometry and Beam Radius

In Fig. 1, we show the general coaxial-cavity geometry and the assumed realistic magnetostatic field profile normalized to its maximum value B_{max}. The outer cavity wall consists of three smooth sections: a downtaper part, a straight midsection, and an uptaper connected through parabolic smoothing sections of length L_d and L_u, respectively. The corrugated coaxial insert has a constant radius R_{coax} at the downtaper part of the cavity and at the beginning of the midsection is down-tapered with a negative angle φ_{coax}. The design of the insert requires a proper selection for the insert radius R_{coax} and its angle φ_{coax}. A too-large insert radius R_{coax} will suppress the competitors but will introduce a prohibitively high ohmic loading at the inner wall, whereas a small one will leave the competing modes unaffected. A small insert angle φ_{coax} will decrease the quality factor of the competitors only slightly, whereas a too-large one may significantly increase the coupling of the competitors, as will be discussed next. The beam radius R_b at the midsection offers an additional degree of freedom for the design. A small displacement of the beam from its optimal radius (the one corresponding to the maximum coupling factor of the operating mode) may improve the selectivity of the cavity as it can deteriorate significantly the coupling of a competitor.

First, let us consider the mode $TE_{32,20}$ (eigenvalue 105.9) as the second-harmonic operating mode. The cavity radius at the midsection R_{out} is set to 29.71 mm for operation at 170 GHz and the optimal beam-wave coupling occurs at a beam radius $R_b = 9.13$ mm. A first insight into the mode competition that the second-harmonic mode is expected to face from its first-harmonic competitors can be gained from the type of mode diagram shown in Fig. 2. On the horizontal axis, we show the cutoff frequency of the second-harmonic operating mode and its main first-harmonic competitors divided by their harmonic number s. On the vertical axis, we show the generalized coupling factor of the second-harmonic mode (red bar) and its main first-harmonic competitors in a *conventional* cavity without a coaxial insert (bars of other colors). We also note the caustic radius of each mode. We see that $TE_{32,20}$ has a

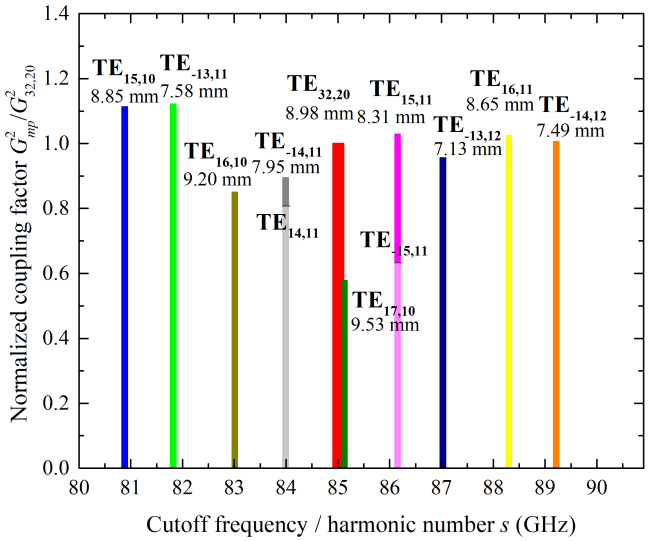

Fig. 2. Main first-harmonic competitors of second-harmonic mode $TE_{32,20}$ in a conventional cavity. The caustic radius of each mode is also noted under its label. The cavity radius is 29.71 mm and $R_b = 9.13$ mm.

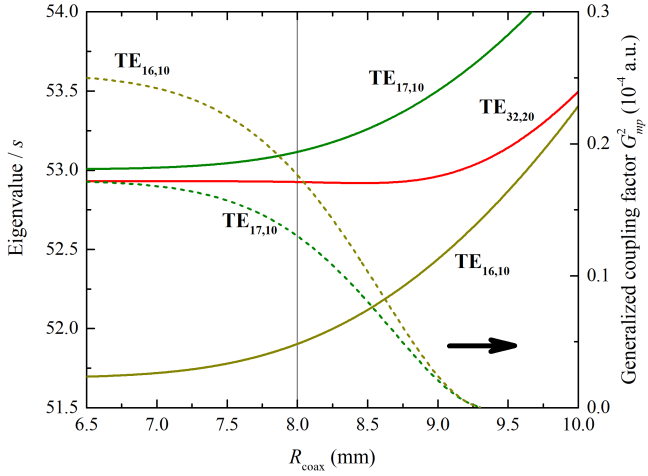

Fig. 3. Eigenvalue (divided by harmonic number s) versus insert radius for the second-harmonic mode $TE_{32,20}$ and the first-harmonic competitors $TE_{16,10}$ and $TE_{17,10}$. The dashed lines correspond to the generalized coupling factor of the competitors. The cavity radius is 29.71 mm.

TABLE I
MULTIMODE SIMULATION RESULTS FOR VARIOUS INSERT PARAMETERS AND OPTIMAL BEAM RADIUS $R_b = 9.13$ mm

φ_{coax}	R_{coax} (mm)	Maximum output power P_{out} (MW)	ρ_{in} (kW/cm^2) at $P_{out} = 2.0$ MW	Dominant competitor
No insert		Not excited	-	$TE_{15,11}$
-1°	8.05	Not excited	-	$TE_{17,10}/TE_{16,10}$
	8.10	Not excited	-	$TE_{16,10}$
	8.15	2.01	1.02	-
-2°	8.05	Not excited	-	$TE_{16,10}$
	8.10	2.05	0.52	-
	8.15	2.09	0.65	-
-3°	8.00	Not excited	-	$TE_{16,10}$
	8.05	1.96	0.28	-
	8.10	2.05	0.33	-
-4°	8.00	Not excited	-	$TE_{17,10}$
	8.05	Not excited	-	$TE_{17,10}$
	8.10	1.96	0.25	-

generalized coupling factor slightly lower than $TE_{15,11}$, which also lies close in frequency, so it is expected that $TE_{15,11}$ will suppress the second-harmonic mode.

In Table I, we present the multimode simulation results for various coaxial insert parameters. The simulations were performed for a cavity midsection length $L_{cav} = 20$ mm, parabolic smoothing lengths $L_d = L_u = 4$ mm, and at the operating point: $B_{max} = 3.505$ T, pitch factor $\alpha = 1.3$, beam current $I_b = 97$ A at beam voltage $V_b = 95$ kV. The midsection length and operating parameters give a normalized interaction length $\mu \cong 20$, which can provide a fair interaction efficiency at the second harmonic [14], [21]. A full diode startup from 60 kV up to 100 kV of beam voltage has been considered including 45 first- and second-harmonic competing modes. In the table, we note the maximum power of the second-harmonic mode, and in case it is not excited, we also note the mode that suppresses it. We also note the ohmic loading at the coaxial insert, which corresponds to an output power of 2.0 MW. If the power is less than 2.0 MW due to mode competition, the noted value corresponds to a single-mode simulation. Note that in all cases of Table I, the outer wall loading was kept below the limit of 2.2 kW/cm^2.

From the first line of Table I, we see that in a conventional hollow cavity without a coaxial insert, indeed, $TE_{15,11}$ suppresses the second-harmonic mode, as expected. Fortunately, $TE_{15,11}$ has a caustic radius of 8.31 mm, which is significantly lower than the caustic radius of the second-harmonic operating mode (8.98 mm). This means that it can be suppressed by a coaxial insert without affecting the operating mode. Indeed, from Table I, we can see that by introducing a coaxial insert with an angle as small as $-1°$, we can easily suppress $TE_{15,11}$.

Despite the suppression of $TE_{15,11}$, now $TE_{17,10}$ and $TE_{16,10}$ take the lead and still suppress the second-harmonic mode. For small insert angles, we see that larger insert radii are required to suppress these modes, resulting in prohibitively high ohmic loading at the insert. Their caustic radius is larger than the operating mode's, so one would expect that they cannot be suppressed by an insert without affecting significantly the operating mode and hence resulting in an unacceptable ohmic loading at the insert. However, this is actually not true as can be seen in Fig. 3, where we plot the eigenvalue of $TE_{32,20}$ and its insisting competitors $TE_{16,10}$ and $TE_{17,10}$ with respect to the insert radius. It is apparent that the first-harmonic competitors are affected first, at smaller insert radii than $TE_{32,20}$ (i.e., around 8.0 mm), despite their higher caustic radii. This effect has to do with the fact that the first-harmonic competitors have twice the wavelength compared to $TE_{32,20}$, so they "feel" the coaxial insert at lower radii compared to $TE_{32,20}$. We can therefore take advantage of this effect to suppress these modes with the insert, too, without affecting a lot the operating mode.

To achieve the excitation of the second-harmonic mode with an acceptable inner ohmic loading, we can increase the slope of the coaxial insert. The effect of a larger (negative) angle φ_{coax} is lower diffractive quality factors for the competitors, which can be thus suppressed without increasing too much the ohmic loading at the insert. Indeed, with an angle of $-4°$,

TABLE II
MULTIMODE SIMULATION RESULTS FOR VARIOUS INSERT PARAMETERS AND LOWER BEAM RADIUS THAN OPTIMAL $R_b = 9.03$ mm

φ_{coax}	R_{coax} (mm)	Maximum output power P_{out} (MW)	ρ_{in} (kW/cm^2) at $P_{out} = 2.0$ MW	Dominant competitor
No insert		Not excited	-	$TE_{15,11}$
	8.00	Not excited	-	$TE_{14,11}$
-1°	8.05	1.94	0.71	-
	8.10	2.01	0.84	-
	7.90	Not excited	-	$TE_{16,10}$
-2°	7.95	2.00	0.27	-
	8.00	2.02	0.34	-
	7.90	Not excited	-	$TE_{16,10}$
-3°	7.95	1.96	0.17	-
	8.00	2.01	0.22	-
	7.95	Not excited	-	$TE_{16,10}$
-4°	8.00	1.96	0.16	-
	8.05	2.01	0.20	-
	8.00	Not excited	-	$TE_{16,10}$
-5°	8.05	1.97	0.15	-
	8.10	2.03	0.19	-
	8.05	Not excited	-	$TE_{16,10}$
-6°	8.10	1.96	0.16	-
	8.15	2.01	0.20	-

we can excite the second-harmonic mode with an acceptable inner loading of 0.25 kW/cm^2. Now, because of the increased angle, the maximum ohmic loading at the insert does not occur in the midsection center (as the field maximum and the ohmic loading at the outer wall), but moves to the left toward the beginning of the midsection. We also note that the taper angle of the coaxial insert cannot be increased arbitrarily for two reasons. First, if the angle of the down-tapered insert exceeds 6°, mode conversion to other radial modes may become significant [22]. Second and more important, with an increased negative angle (and for a constant insert radius R_{coax}), the local insert radius at the center of the midsection decreases. The coupling of the competitors is then improved as can be seen in Fig. 3, where we also show the generalized coupling factor of $TE_{16,10}$ and $TE_{17,10}$ versus the insert radius (dashed lines). For (negative) angles higher than 4°–5°, this effect overwhelms the reduced quality factors and the mode competition becomes stronger.

One way to further decrease the inner ohmic loading at safer levels and enhance the stability of the design is to position the beam not at the operating mode's optimal coupling, but at a slightly lower radius. The first-harmonic competitors, in general, have an optimal coupling at larger radii than the second-harmonic operating mode due to the term $J_{m-s}(k_\perp R_b)$, which for comparable caustic radii gives a first maximum at lower beam radii for the second-harmonic mode ($s = 2$) than for its first-harmonic competitors ($s = 1$). As a result, for a beam radius slightly smaller than the one that gives optimal coupling, the coupling of the operating second-harmonic mode decreases only slightly, since we are close to the maximum and the gradient is small, whereas for the main first-harmonic competitors, the coupling deteriorates to a much larger extent.

In Table II, we present the simulation results for a beam radius $R_b = 9.03$ mm, which is slightly lower than the optimal one ($R_b = 9.13$ mm). For each simulation, one should take

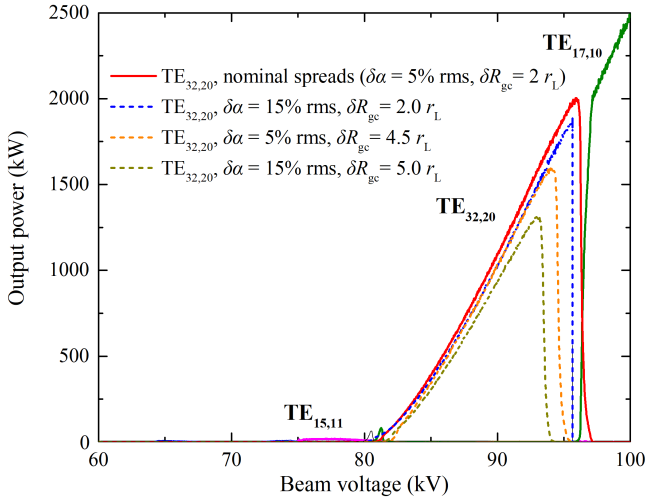

Fig. 4. Output power versus voltage of multimode simulation showing second-harmonic excitation of $TE_{32,20}$ at 2.0 MW. $R_{out} = 29.71$ mm, $R_b = 9.03$ mm, $R_{coax} = 8.1$ mm, $\varphi_{coax} = -5°$. The main first- and second-harmonic competitors are included (45 modes).

care to update the list of competitors, taking into account the updated beam radius and coaxial insert parameters. Again, in all cases of Table II, the outer wall loading was kept below the limit of 2.2 kW/cm^2. We see in Table II that the results are significantly improved compared to those with the optimal beam radius (Table I). The second-harmonic mode can be excited at lower insert radii, which imply a much lower ohmic loading at the insert. We also see that the beneficial effect of a large insert slope saturates at about −5°. The best performance is achieved for this slope and $R_{coax} = 8.10$ mm; the output power is above 2.0 MW (shown in Fig. 4) and the electronic efficiency is 22%. The outer and inner ohmic loading are 2.05 and 0.19 kW/cm^2, respectively, i.e., within the limits.

Summarizing the above design considerations, we have shown that: 1) the coaxial insert can effectively suppress the first-harmonic competitors with lower caustic radii; 2) the coaxial insert can also suppress the modes that have caustic radii that are even larger than the operating mode's, without affecting significantly the operating second-harmonic mode, owing to the longer wavelength of the first-harmonic competitors; 3) a larger taper angle up to about −5° is beneficial because the quality factors of the first-harmonic competitors decrease further. Larger (negative) angles are not beneficial because the improvement in the coupling of the competitors overwhelms the lower quality factors; and 4) finally, a slightly lower beam radius can improve further the competition, since the optimal coupling of the main first-harmonic competitors occurs at a larger beam radius than the one of the second-harmonic mode.

III. CAVITY DESIGNS WITH OTHER OPERATING MODES

We consider now some other operating modes of the same eigenvalue level (namely $TE_{31,20}$, $TE_{29,21}$, $TE_{34,19}$), which exhibit a different placing among their first-harmonic competitors with respect to cutoff frequency and coupling factor. This could imply a different behavior as regards mode competition. However, as shown in Table III, the achieved performance of

TABLE III
PERFORMANCE OF CAVITY DESIGNS FOR DIFFERENT MODES

Mode	Eigenvalue	Output Power (MW)	ρ_{out} (kW/cm^2)	ρ_{in} (kW/cm^2)	Efficiency (%)
$TE_{32,20}$	105.9	2.0	2.05	0.19	22
$TE_{31,20}$	104.5	2.0	2.16	0.19	22
$TE_{29,21}$	105.1	2.0	2.14	0.24	22
$TE_{34,19}$	105.2	2.0	2.14	0.18	22

all examined modes is quite similar, at the level of 2.0 MW output power and 22% efficiency. The operating point, cavity length, parabolic smoothing lengths, and design considerations are exactly the same as for $TE_{32,20}$ considered in Section II.

The cavity designs of Table III have been simulated also with increased beam spreads. All designs were found to be quite stable with respect to high velocity-spread values. The operating mode was excited up to at least 15% rms spread in velocity ratio α, giving, however, a reduced power level of about 7%. The designs for $TE_{34,19}$, $TE_{32,20}$, and $TE_{31,20}$ are also robust against increased guiding center spreads up to about a uniform spread of about $6.0r_L$, $5.0r_L$, and $4.5r_L$, where r_L is the Larmor radii: the second-harmonic mode is still excited but at reduced power level, as expected. Only $TE_{29,21}$ was found more sensitive to guiding center spreads as was stably excited only for a uniform spread of up to three Larmor radii. In conclusion, different modes do not seem to have large differences as regards mode competition, since the examined modes exhibit more or less the same performance. We note also that designing efficient quasi-optical systems for the considered high-order modes should not be a problem as this already has been done for $TE_{34,19}$, which has achieved a measured Gaussian content of 96% [13].

IV. CAVITY DESIGN FOR 280 GHZ

MW-class operation at a frequency as high as 280 GHz poses a significant challenge, especially at the second harmonic. The ohmic losses increase significantly at 280 GHz (for a given mode, they scale with frequency as $f^{5/2}$) and to keep the ohmic loading below the technological limit, the field amplitude inside the cavity has to be reduced compared to 170 GHz. This has a negative impact both on the output power and the interaction efficiency. We have already shown that we can excite second-harmonic modes with eigenvalues in the order of 105. For 280 GHz, we choose the mode $TE_{35,20}$, which has a more whispering-gallery character (caustic radius 6.0 mm in a cavity for operation at 280 GHz) than the modes considered for 170 GHz. This is a necessary choice because a design for the modes considered in Section III would lead to a very thin coaxial insert with a diameter in the order of 8 mm, which would be difficult to manufacture in a way that supports CW operation with active cooling.

Following the general principles described in Section II, we arrived at a design with geometrical parameters: $L_{cav} = 13.5$ mm ($\mu \cong 21$), $R_{cav} = 18.70$ mm, $R_{coax} = 5.55$ mm, $R_b = 6.02$ mm, $L_d = 4$ mm, $L_d = 4.6$ mm, $\varphi_{coax} = -5°$ at the operating point $B_{max} = 5.66$ T, $I_b = 64$ A, $\alpha = 1.33$, and $V_b = 78$ kV. In this way, we managed to suppress all first- and

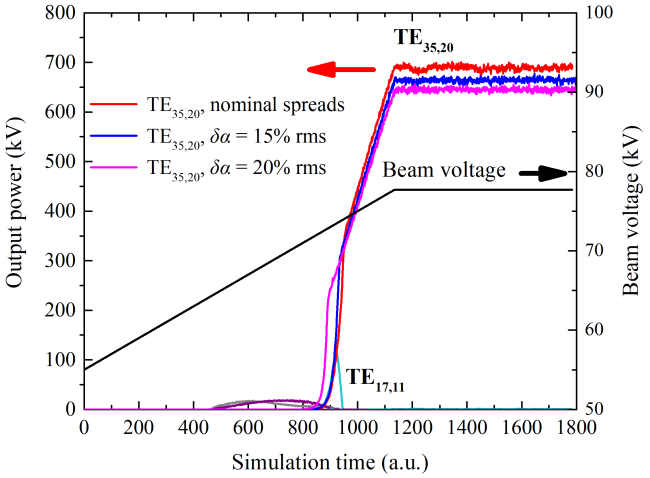

Fig. 5. Simulated output power and beam voltage versus time for the 280 GHz second-harmonic coaxial-cavity design. The voltage rises from 55 kV up to the operating voltage of 77.7 kV; 54 modes have been considered.

second-harmonic competitors and excite $TE_{35,20}$ at the second harmonic. The achieved performance is 0.7 MW of output power at the cavity exit and 15% electronic efficiency with outer ohmic loading of 2.15 kW/cm^2 and inner ohmic loading of 0.33 kW/cm^2. The stable excitation of the second-harmonic mode is shown in Fig. 5. The 15% electronic efficiency can be enhanced to 47% of total efficiency with a multistage depressed collector (assuming a collector efficiency of 80%). For comparison purposes with respect to first-harmonic results, we mention the design at 240 GHz [23] and the experiment at 250 GHz [24], in which the output power is 1 MW and 330 kW, respectively.

The cavity was also simulated with increased beam spreads and was found robust against high spread values in the electron velocity ratio α of 10%, 15%, and 20% rms, giving reduced power by 10, 30, and 50 kW, respectively. For higher values of the velocity spread, the mode did not get excited. The cavity design was found more sensitive to guiding center spreads as it was found stable only up to a uniform spread of 2.4 Larmor radii. One possible concern for this specific design and in general for other high-frequency designs is the proximity of the electron beam to the coaxial insert. In our design, the minimum distance is 0.48 mm, which corresponds to about 3.5 Larmor radii. If this clearance is found not to be safe, one could try to use a counter-rotating mode as the operating one, since it exhibits a larger optimal radius than the corresponding co-rotating mode, but in this case, a slightly reduced performance is expected due to the lower coupling. In general, a MW-class high-frequency design presents a significant challenge with respect to precision manufacturing, alignment, and beam positioning due to the short wavelength.

V. CONCLUSION

We have investigated the possibility for high-frequency MW-class gyrotrons operating at the second harmonic of the electron cyclotron frequency. A coaxial cavity with a corrugated insert was used to overcome the intense problem of mode competition from the first-harmonic competitors. Specific second-harmonic cavity designs for very high-order

modes with eigenvalues above 100 have been developed for 170 and 280 GHz. The achieved performance is 2.0 MW output power with 22% electronic efficiency for 170 GHz and 0.7 MW power with 15% efficiency for 280 GHz.

For the operation to be CW-compatible in all cases, the ohmic loading was kept below 2.2 kW/cm^2 for the outer wall as well as below 0.39 kW/cm^2 for the inner wall, as proposed in [19]. However, as there has been no experimental demonstration of CW operation for a MW-class coaxial gyrotron up to now, there is some uncertainty on the real limitation for the insert loading. In relevance to this, it should be mentioned that an alternative method for enhancing the suppression of the first-harmonic competing modes is investigated in [25] using mode-converting corrugation on the outer cavity wall. It is shown that with this method, the loading on the insert could be somewhat relaxed, albeit with increased complexity of the cavity geometry.

The above results show the possibility of operating gyrotrons at the second harmonic and achieving MW-class output power at high frequencies through the use of a coaxial cavity with a smooth outer wall and corrugated insert, a concept that has already been experimentally verified for short-pulse operation at the first harmonic. This allows the use of the existing cost-effective magnet technology for generating MW-class microwave radiation at frequencies higher than 250 GHz.

Acknowledgment

Part of the simulations was performed on the EUROfusion High Performance Computer (Marconi-Fusion). The authors would like to thank Lukas Feuerstein for his valuable comments on the article.

References

[1] M. K. A. Thumm, G. G. Denisov, K. Sakamoto, and M. Q. Tran, "High-power gyrotrons for electron cyclotron heating and current drive," *Nucl. Fusion*, vol. 59, no. 7, Jun. 2019, Art. no. 073001, doi: 10.1088/1741-4326/ab2005.

[2] D. G. Whyte, J. Minervini, B. LaBombard, E. Marmar, L. Bromberg, and M. Greenwald, "Smaller & sooner: Exploiting high magnetic fields from new superconductors for a more attractive fusion energy development path," *J. Fusion Energy*, vol. 35, no. 1, pp. 41–53, Jan. 2016, doi: 10.1007/s10894-015-0050-1.

[3] A. J. Creely et al., "SPARC as a platform to advance tokamak science," *Phys. Plasmas*, vol. 30, no. 9, Sep. 2023, Art. no. 090601, doi: 10.1063/5.0162457.

[4] T. Saito et al., "Developments for collective Thomson scattering equipment with a sub-THz gyrotron in LHD," in *Proc. EPJ Web Conf.*, vol. 203, Mar. 2019, p. 03012, doi: 10.1051/epjconf/201920303012.

[5] Y. Tatematsu et al., "Development of second harmonic gyrotrons, gyrotron FU CW GII and gyrotron FU CW GIII, equipped with internal mode converters," *J. Infr., Millim., Terahertz Waves*, vol. 35, no. 2, pp. 169–178, Jan. 2014, doi: 10.1007/s10762-014-0048-1.

[6] S. K. Jawla, R. G. Griffin, I. A. Mastovsky, M. A. Shapiro, and R. J. Temkin, "Second harmonic 527-GHz gyrotron for DNP-NMR: Design and experimental results," *IEEE Trans. Electron Devices*, vol. 67, no. 1, pp. 328–334, Jan. 2020, doi: 10.1109/TED.2019.2953658.

[7] M. Blank, P. Borchard, S. Cauffman, K. Felch, M. Rosay, and L. Tometich, "High-frequency gyrotrons for DNP-enhanced NMR applications," in *Proc. IEEE Int. Vac. Electron. Conf.*, Monterey, CA, USA, Apr. 2014, pp. 7–8, doi: 10.1109/IVEC.2014.6857463.

[8] M. Y. Glyavin et al., "A 250-watts, 0.5-THz continuous-wave second-harmonic gyrotron," *IEEE Electron Device Lett.*, vol. 42, no. 11, pp. 1666–1669, Nov. 2021, doi: 10.1109/LED.2021.3113022.

[9] T. Notake et al., "Development of a novel high power sub-THz second harmonic gyrotron," *Phys. Rev. Lett.*, vol. 103, no. 22, Nov. 2009, Art. no. 225002, doi: 10.1103/physrevlett.103.225002.

[10] G. G. Denisov et al., "Phase-locking of second-harmonic gyrotrons for providing MW-level output power," *IEEE Trans. Electron Devices*, vol. 69, no. 2, pp. 754–758, Feb. 2022, doi: 10.1109/TED.2021.3134187.

[11] C. T. Iatrou, S. Kern, and A. B. Pavelyev, "Coaxial cavities with corrugated inner conductor for gyrotrons," *IEEE Trans. Microw. Theory Techn.*, vol. 44, no. 1, pp. 56–64, Jan. 1996, doi: 10.1109/22.481385.

[12] C. T. Iatrou, "Mode selective properties of coaxial gyrotron resonators," *IEEE Trans. Plasma Sci.*, vol. 24, no. 3, pp. 596–605, Jun. 1996, doi: 10.1109/27.532942.

[13] T. Rzesnicki et al., "2.2-MW record power of the 170-GHz European preprototype coaxial-cavity gyrotron for ITER," *IEEE Trans. Plasma Sci.*, vol. 38, no. 6, pp. 1141–1149, Jun. 2010, doi: 10.1109/TPS.2010.2040842.

[14] K. A. Avramides, C. T. Iatrou, and J. L. Vomvoridis, "Design considerations for powerful continuous-wave second-cyclotron-harmonic coaxial-cavity gyrotrons," *IEEE Trans. Plasma Sci.*, vol. 32, no. 3, pp. 917–928, Jun. 2004, doi: 10.1109/TPS.2004.828781.

[15] V. I. Shcherbinin, "Multifunctional coaxial insert with distributed impedance corrugations for cavities of broadband tunable second-harmonic gyrotrons," *IEEE Trans. Electron Devices*, vol. 68, no. 8, pp. 4104–4109, Aug. 2021, doi: 10.1109/TED.2021.3090348.

[16] V. I. Shcherbinin, Y. K. Moskvitina, K. A. Avramidis, and J. Jelonnek, "Improved mode selection in coaxial cavities for subterahertz second-harmonic gyrotrons," *IEEE Trans. Electron Devices*, vol. 67, no. 7, pp. 2933–2939, Jul. 2020, doi: 10.1109/TED.2020.2996179.

[17] L. Feuerstein, A. Marek, C. Wu, S. Illy, M. Thumm, and J. Jelonnek, "Design of a second harmonic MW-level coaxial gyrotron cavity," in *Proc. IEEE Int. Vac. Electron. Conf. (IVEC)*, Chengdu, China, Apr. 2023, pp. 1–2, doi: 10.1109/IVEC56627.2023.10156958.

[18] B. F. Ell et al., "Toward the first continuous wave compatible multistage depressed collector design for high power gyrotrons," *IEEE Trans. Electron Devices*, vol. 70, no. 3, pp. 1299–1305, Mar. 2023, doi: 10.1109/TED.2023.3234885.

[19] P. C. Kalaria et al., "Multiphysics modeling of insert cooling system for a 170-GHz, 2-MW long-pulse coaxial-cavity gyrotron," *IEEE Trans. Electron Devices*, vol. 66, no. 9, pp. 4008–4015, Sep. 2019, doi: 10.1109/TED.2019.2928222.

[20] K. A. Avramides, I. G. Pagonakis, C. T. Iatrou, and J. L. Vomvoridis, "EURIDICE: A code-package for gyrotron interaction simulations and cavity design," in *Proc. EPJ Web Conf.*, vol. 32, Sep. 2012, p. 04016, doi: 10.1051/epjconf/20123204016.

[21] B. G. Danly and R. J. Temkin, "Generalized nonlinear harmonic gyrotron theory," *Phys. Fluids*, vol. 29, no. 2, pp. 561–567, Feb. 1986, doi: 10.1063/1.865446.

[22] E. Borie and O. Dumbrajs, "Calculation of eigenmodes of tapered gyrotron resonators," *Int. J. Electron.*, vol. 60, no. 2, pp. 143–154, Feb. 1986, doi: 10.1080/00207218608920768.

[23] N. Kumar, U. Singh, A. Bera, and A. K. Sinha, "RF behavior of cylindrical cavity based 240 GHz, 1 MW gyrotron for future tokamak system," *J. Infr., Millim., Terahertz Waves*, vol. 38, no. 11, pp. 1342–1356, Nov. 2017, doi: 10.1007/s10762-017-0419-5.

[24] G. G. Denisov et al., "First experimental tests of powerful 250 GHz gyrotron for future fusion research and collective Thomson scattering diagnostics," *Rev. Sci. Instrum.*, vol. 89, no. 8, Aug. 2018, Art. no. 084702, doi: 10.1063/1.5040242.

[25] D. V. Peponis et al., "Design of MW-class coaxial gyrotron cavities with mode-converting corrugation operating at the second cyclotron harmonic," *IEEE Trans. Electron Devices*, vol. 70, no. 12, pp. 6587–6593, Dec. 2023, doi: 10.1109/TED.2023.3326431.